

Article

# Pollution Characteristics, Chemical Compositions, and Population Health Risks during the 2018 Winter Haze Episode in Jiangnan Plain, Central China

Huimeng Jiang <sup>1</sup>, Xiaowei Lei <sup>1</sup>, Han Xiao <sup>1</sup>, Danhong Chen <sup>1</sup>, Pei Zeng <sup>1</sup>, Xingyun Yang <sup>2</sup>, Zuwu Wang <sup>1,\*</sup> and Hairong Cheng <sup>1,\*</sup>

<sup>1</sup> School of Resource and Environmental Sciences, Wuhan University, Wuhan 430072, China; hjgcapc2014@whu.edu.cn (H.J.); leixiaowei@whu.edu.cn (X.L.); han\_xiao@cas-pe.com (H.X.); 2014301110152@whu.edu.cn (D.C.); zengp@whu.edu.cn (P.Z.)

<sup>2</sup> Xiantao Municipal Ecological Environment Bureau, Xiantao 433000, China; 15871918541@126.com

\* Correspondence: zwwang@whu.edu.cn (Z.W.); chenghr@whu.edu.cn (H.C.)

Received: 26 August 2020; Accepted: 4 September 2020; Published: 7 September 2020



**Abstract:** To determine the pollution characteristics, chemical compositions, and population health risks of PM<sub>2.5</sub> at different pollution levels, PM<sub>2.5</sub> samples were intensively collected during the long-lasting winter haze episode from 13–23 January 2018 in Xiantao in Jiangnan Plain (JHP), central China. The higher PM<sub>2.5</sub> levels during the severe pollution period were dominated by the WNW–NNE air-masses, whereas the lower PM<sub>2.5</sub> concentrations during other pollution periods were mainly affected by the NE, S, and NW air-masses. The NO<sub>3</sub><sup>−</sup>/SO<sub>4</sub><sup>2−</sup> and OC/EC ratios indicated a mixed contribution of intensive vehicle exhaust and secondary formation. The enrichment factor and geo-accumulation index for assessing the PM<sub>2.5</sub>-bound metal(loid)s contamination levels were positively correlated. Ingestion is the dominant exposure pathway of PM<sub>2.5</sub>-bound metal(loid)s for children and adults, followed by inhalation and dermal contact. As, Cr, and Pb may pose carcinogenic and non-carcinogenic risks, whereas Sb and V may only pose non-carcinogenic risks for children and adults. The population health risks may not depend on the pollution levels but depend on the PM<sub>2.5</sub>-bound metal(loid)s concentrations. PM<sub>2.5</sub>-bound metal(loid)s may pose much higher population health risks for adults compared to children. More attentions should be paid to the population health risks of PM<sub>2.5</sub>-bound metal(loid)s during a long-lasting winter haze episode in JHP.

**Keywords:** PM<sub>2.5</sub>; winter haze episode; metal(loid)s; population health risk; Xiantao; Jiangnan Plain

## 1. Introduction

Haze is associated with the explosive growth of airborne fine particulate matter (PM<sub>2.5</sub>) in ambient air [1]. PM<sub>2.5</sub> has attracted worldwide concerns over the several years because of its adverse effects on atmospheric visibility and human health [2]. For example, PM<sub>2.5</sub> can deposit in lungs through the inhalation exposure pathway and then result in lung cancer and acute respiratory infections [3]. In addition, it was classified as belonging to cancerogenic substance Group I by the International Agency for Research on Cancer [4]. However, the impacts of PM<sub>2.5</sub> on population health rely on its chemical compositions, such as metal(loid)s, which represent all kinds of PM<sub>2.5</sub>-bound metals and metalloids [5], and organic components [6]. It was reported that PM<sub>2.5</sub>-bound metal(loid)s have influences on acute changes in cardiorespiratory physiology [7] and allergic airways disease [8], whereas PM<sub>2.5</sub>-bound elemental carbon is the main contributor to epidemiological disease [9]. Hence, necessary knowledge of PM<sub>2.5</sub> chemical compositions is beneficial for the public and government to evaluate the population health risks.

Several studies have investigated the pollution characteristics and chemical compositions of PM<sub>2.5</sub> in China, including Xi'an [10], Beijing-Tianjin-Hebei Region [11,12], Nanjing [13], Shanghai [14], Chengdu [15], Zhengzhou [16], Wuhan [17], and Xiangyang [18]. However, information regarding PM<sub>2.5</sub> dynamic variations in Jiangnan Plain (JHP), central China has not yet been reported so far. The study related to ambient air in JHP has focused on the spatiotemporal variation of atmospheric organochlorine pesticides [19] and ozone [20]. To our best knowledge, this is first the comprehensive study of the pollution characteristics, chemical compositions, and population health risks of PM<sub>2.5</sub> in JHP, especially during a long-lasting winter haze episode.

JHP is located in the central and southern Hubei Province and is named after the alluvial deposits of the Yangtze River and Han River, where rice, cotton, and rape are mainly planted. With an average altitude of only 27 m, it is an important part of the plains of the middle and lower reaches of the Yangtze River in central China and is identified as a pollution hotspot [20]. Xiantao (30°04'~30°32' N, 112°55'~113°49' E) is a traditional agriculture city in JHP, central China, with an area and population of 2538 km<sup>2</sup> and 1.14 million, respectively. According to the Xiantao Yearbook (<http://tj.hubei.gov.cn/tjsj/sjksxc/tjnj/gszjtj/xts/>), the gross domestic product (GDP) composed of primary industries (10.9%), secondary industries (51.6%), and tertiary industries (37.5%) of Xiantao reached 11.4 billion USD in 2018. These main industries in Xiantao include non-woven, electronic and electrical, textile and clothing, food processing, new materials and pharmaceutical manufacturing, and machinery and automotive parts, which accounted for 26.3%, 5.38%, 9.28%, 17.8%, 11.9%, and 11.6% of the GDP of industries, respectively. Xiantao's car ownership increased from 171,264 in 2017 to 193,614 in 2018 by 13.1%. There are approximately 143 Gg of coal consumption for power plants and 13.5 Gg of coal consumption for residential biofuel, which are potential emission sources of PM<sub>2.5</sub>. According to the statistics of the Environmental Air quality Report of key cities in Hubei Province (<http://sthjt.hubei.gov.cn/fbjd/zwgk/jcsjfb/hjkq/>), the average PM<sub>2.5</sub> concentration in January from 2012–2017 was 123 µg m<sup>-3</sup>, which was 1.64 times than the Grade II of National Ambient Air Quality Standards of China (NAAQS, 75 µg m<sup>-3</sup>) (GB 3095-2012, [https://www.mee.gov.cn/ywgz/fgbz/bz/bzwb/dqhjbh/dqhjzlbz/201203/t20120302\\_224165.shtml](https://www.mee.gov.cn/ywgz/fgbz/bz/bzwb/dqhjbh/dqhjzlbz/201203/t20120302_224165.shtml)), indicating a heavy PM<sub>2.5</sub> pollution during wintertime in JHP, central China. As reported in Environmental Quality Bulletin of Xiantao City in 2018 (<http://hbj.xiantao.gov.cn/hjzl/hjzlggg/201908/P020200102465288147981.pdf>), the frequency of haze events in this region is 26.8% in 2018. In January 2018, the frequency of haze events in this region is 50.2%. This makes it urgent for the government and public to take insight into the pollution characteristics, chemical compositions, and population health risks of PM<sub>2.5</sub> for mitigating the haze episode in JHP.

In this study, a total of 43 pairs of PM<sub>2.5</sub> samples were effectively collected during the long-lasting winter haze episode from 13–23 January 2018 in Xiantao in JHP, central China. The objectives of this study were to: (1) analyze the pollution characteristics, chemical compositions of PM<sub>2.5</sub>, including water-soluble inorganic ions (WSIIs), carbonaceous species (CAs), and trace elements (TE); (2) evaluate the contamination levels of PM<sub>2.5</sub>-bound metal(loid)s; (3) assess the population health carcinogenic and non-carcinogenic risks for children and adults due to exposure to PM<sub>2.5</sub>-bound metal(loid)s through ingestion, inhalation, and dermal contact pathways. This study provides important information for population health risks posed by PM<sub>2.5</sub>-bound metal(loid)s at four different pollution levels of Xiantao, which has a great praxis function as a reference for other cities in JHP, central China.

## 2. Materials and Methods

### 2.1. Field Sampling Campaign

According to the forecast results of Regional Air Quality Forecast System (<http://aqf.climblue.com/>) based on the Weather Research and Forecasting - Community Multiscale Air Quality (WRF-CMAQ) model provided by the International Institute for Earth System Science, Nanjing University, there would be a long-lasting winter haze episode from 13 January 2018 in Hubei Province, especially in Xiangyang,

Jingmen, Wuhan, and Xiantao. Therefore, we conducted the intensive sampling campaign in 13 January 2018. PM<sub>2.5</sub> field sampling campaign was carried out at an urban site from 13–23 January 2018 in Xiantao in JHP, central China. The geographical location of this sampling site is plotted in Figure 1. There is no obvious pollution source which may have effect on the sampling work around this urban sampling site, because the scale of industries near the sampling site, such as Ruiyang Automotive Parts (Xiantao) Co. Ltd. and Xiangyuan Electromechanical Equipment Co. Ltd. (Xiantao, China), are very small or do not have an independent production process. To track the haze bloom–decay process, samples were simultaneously collected on the rooftop of the library of Xiantao Vocational College (~20 m height, 30°20′27″ N, 113°25′16″ E) four times a day (at local times 06:00–11:00, 11:30–16:30, 17:00–22:00, and 22:30–05:30 the following day) with two medium-volume samplers (TH-150F, Wuhan Tianhong Instrument Co., Ltd., Wuhan, China) at an air flow rate of 100 L min<sup>-1</sup> to increase the number of PM<sub>2.5</sub> samples classified at different pollution levels as much as possible. This prevented the stoppage of sampling due to excessive filter resistance caused by a haze episode. However, heavy rains and snowy weather were observed from the evening of 23 January till 27 January 2018. So, we terminated this intensive sampling process on 24 January 2018 after the fourth sample collection was completed on 22:30 23 January–05:30 24 January 2018. To subtract possible contamination occurring during or after sampling, blank samples were collected for about 20 min by mounting blank filters onto the samplers without pumping into any air separately before and after the sampling [21]. In sum, a total of 43 pairs of PM<sub>2.5</sub> samples as well as three pairs of blank samples were effectively collected on quartz fiber filters (Whatman, UK) and Teflon filters (Munktell, Sweden), respectively. The sample data on 06:00–11:00 21 January was missing because the power supply line was cut off by accident, which meant that the two samplers could not work normally during this period. The quartz fiber filters were baked at 500 °C for 6 h in a muffle furnace and the Teflon filters were prepared at a constant temperature and relative humidity (25 ± 1 °C, 50 ± 5%) for 48 h before use, respectively. An electronic microbalance with a resolution of 1 µg (Sartorius SECURA 125-1S, Sartorius Lab Instruments GmbH & Co. KG, Göttingen, Germany) was used to determine the PM<sub>2.5</sub> mass on Teflon filters. After sampling, all the quartz fiber filters folded, wrapped with aluminum foil, then were sealed in plastic bags, and finally were stored in a refrigerator at -18 °C as well as Teflon filters for chemical analysis. According to the Technical Regulation on Air Quality Index of China (HJ 633-2012, [http://www.mee.gov.cn/gkml/hbb/bgg/201203/t20120302\\_224146.htm](http://www.mee.gov.cn/gkml/hbb/bgg/201203/t20120302_224146.htm)), the sampling periods were divided into four pollution levels: mild, moderate, heavy, and severe pollution when the PM<sub>2.5</sub> concentrations were between 75 and 115, 115 and 150, 150 and 250, and greater than 250 µg m<sup>-3</sup>, respectively. The sample numbers for mild pollution, moderate pollution, heavy pollution, and severe pollution levels are 17, 10, 10, and 3, respectively.

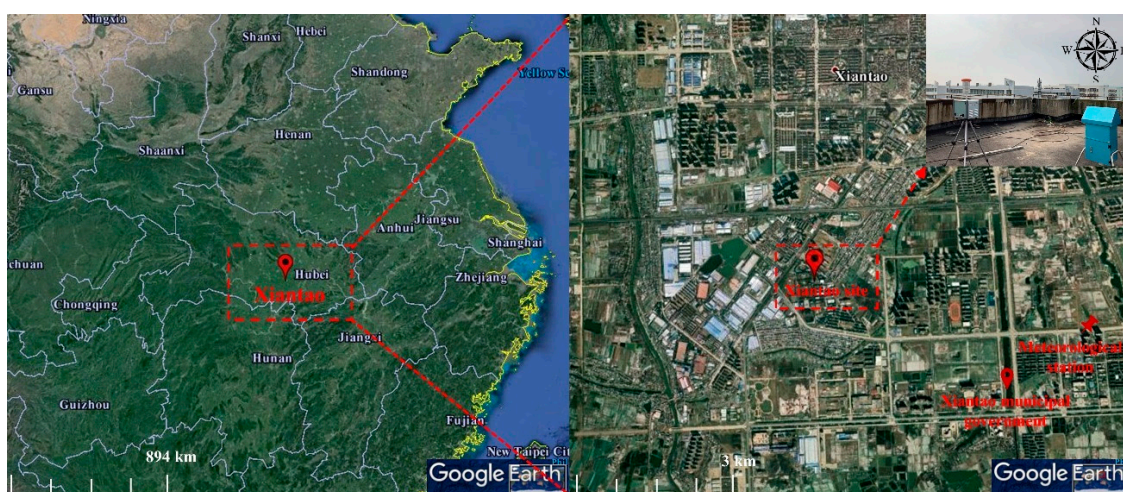


**Figure 1.** The geographical location of Xiantao sampling site (© Google Earth).

## 2.2. Chemical Analysis

The analysis method and procedures of WSIs, CAs, and TE have been described in our previous studies [22–25]. To determine the WSIs, a punch (3.14 cm<sup>2</sup>) of quartz fiber filter was extracted using 20 mL ultrapure Milli-Q water (18.25 MΩ cm). After 45 min ultrasonic ice-water bath extraction, the solution was filtered through a 0.22 μm pore size hydrophilic filter and then stored in a clean HDPE bottle. Nine WSIs in the extraction solution, including four anions (F<sup>-</sup>, Cl<sup>-</sup>, NO<sub>3</sub><sup>-</sup>, and SO<sub>4</sub><sup>2-</sup>) and five cations (Na<sup>+</sup>, NH<sub>4</sub><sup>+</sup>, K<sup>+</sup>, Mg<sup>2+</sup>, and Ca<sup>2+</sup>), were measured using an Ion Chromatography (883 Basic IC plus, Metrohm, Switzerland). The detection limits of F<sup>-</sup>, Cl<sup>-</sup>, NO<sub>3</sub><sup>-</sup>, SO<sub>4</sub><sup>2-</sup>, Na<sup>+</sup>, NH<sub>4</sub><sup>+</sup>, K<sup>+</sup>, Mg<sup>2+</sup>, and Ca<sup>2+</sup> were 0.010, 0.012, 0.027, 0.030, 0.019, 0.020, 0.025, 0.020, and 0.037 μg m<sup>-3</sup>, respectively. The OC and EC were analyzed using a thermal/optical reflectance carbon analyzer (DRI 2001 A, Desert Research Institute, USA). Briefly, a punch (0.518 cm<sup>2</sup>) of quartz fiber filter was stepwise heated at 140 °C (OC1), 280 °C (OC2), 480 °C (OC3), and 580 °C (OC4) in a pure He gas atmosphere for OC volatilization and at 580 °C (E1), 740 °C (E2), and 840 °C (E3) in a 2% O<sub>2</sub>/98% He atmosphere for EC oxidation for 150 s at each stage in the oven. The differences from replicate analyses on 10% of the total samples were within 3.95% for OC and 2.53% for EC. Standard concentrations of CH<sub>4</sub>/CO<sub>2</sub> mixed gases were used to calibrate the analyzer each day. TE was measured using an Inductively Coupled Plasma-Mass Spectrometer (ICP-MS, PerkinElmer 350D, Boston, USA). Briefly, a Teflon filter was digested with a 10 mL acid mixture of 68% HNO<sub>3</sub> and 40% HF (1:1, *v/v*) in a microwave system for 45 min. The digested solution was filtered through a 0.22 μm pore size hydrophilic filter after it cooled to room temperature and then was measured to determine the mass concentrations of twenty-five TE, including Li, Be, Al, Si, V, Cr, Mn, Co, Ni, Cu, Zn, As, Se, Sr, Mo, Ag, Cd, Sn, Sb, Ba, Tl, Pb, Bi, Th, and U. The relative standard deviations of soil national standard materials real values (Sigma-Aldrich, Saint Louis, USA) ranged from 0.10 to 18.00%. The detection limits of TE ranged from 0.00001 to 0.0005 μg L<sup>-1</sup>. Analyses of filed blank samples were performed using the above same methods. All the reported data of WSIs, CAs, and TE were corrected by the field blanks.

## 2.3. Data Analysis Methods

### 2.3.1. Meteorological Parameters, Trace Gases, and Air Mass Back Trajectory Analysis

Hourly meteorological parameters in January 2018 (Supplementary Figure S1), including wind direction (WD), wind speed (WS), temperature (Temp.) relative humidity (RH), precipitation (Prec.), and visibility (Vis.) were collected from the nearest meteorological station to the sampling site (3 km, Figure 1), which can represent the ambient meteorology for the Xiantao site. Trace gases (Supplementary Figure S2), including SO<sub>2</sub> and NO<sub>2</sub>, during the sampling time at Xiantao site were collected from the same place of Xiantao Industrial Park Station, which is a provincial controlled air quality monitoring station. To determine the long-range transport of air masses from different potential regions, 3 days (72 h) air mass back trajectories were calculated every 4 h (00:00, 06:00, 12:00, and 18:00 UTC) at 500 m A.G.L and were cross-checked at 1000 m A.G.L using the hybrid single particle Lagrangian integrated trajectory (HYSPLIT) model (<https://www.arl.noaa.gov/hysplit/>), provided by the US NOAA. All the air mass back trajectories were clustered into four typical types, including NW (20%), S (24%), WNW-NNE (50%), and NE (7%), by HYSPLIT 4.8 and GIS 10.2 software using a hierarchical clustering method.

### 2.3.2. Geo-Accumulation Index

To compare the concentration of PM<sub>2.5</sub>-bound metal(loid)s in ambient air with the concentration in the earth's crust, the geo-accumulation index (*I*<sub>Geo</sub>) was used to evaluate contamination levels of metal(loid)s in PM<sub>2.5</sub> aerosol samples [26] as follows:

$$I_{Geo} = \log_2 \frac{C_{iAerosol}}{(1.5 \times C_{iCrust})}, \quad (1)$$

where  $C_{i_{\text{Aerosol}}}$  and  $C_{i_{\text{Crust}}}$  represent the concentration of measured metal(loid) 'i' in the PM<sub>2.5</sub> aerosol samples and the earth's crust, respectively. The background metal(loid)s concentrations ( $C_{i_{\text{Crust}}}$ ) of Li, Be, V, Cr, Mn, Co, Ni, Cu, Zn, As, Se, Sr, Mo, Ag, Cd, Sn, Sb, Ba, Tl, Pb, Bi, Th, U, and Al of Hubei Province in the earth's crust were  $37.1 \pm 10.2$ ,  $2.09 \pm 0.50$ ,  $110 \pm 41.9$ ,  $86.0 \pm 36.9$ ,  $712 \pm 309$ ,  $15.4 \pm 5.24$ ,  $37.3 \pm 15.0$ ,  $30.7 \pm 14.1$ ,  $83.6 \pm 36.2$ ,  $12.3 \pm 7.31$ ,  $0.28 \pm 0.35$ ,  $116 \pm 80.7$ ,  $1.70 \pm 2.52$ ,  $0.18 \pm 0.11$ ,  $0.17 \pm 0.19$ ,  $2.20 \pm 0.71$ ,  $1.65 \pm 0.61$ ,  $542 \pm 229$ ,  $0.58 \pm 0.10$ ,  $26.7 \pm 7.86$ ,  $0.34 \pm 0.11$ ,  $14.5 \pm 1.60$ ,  $3.20 \pm 1.00 \text{ mg kg}^{-1}$ , and  $7.19 \pm 1.80\%$ , respectively, provided by the Background Values of Soil Elements in China [27]. The constant of 1.5 was to verify the natural fluctuations of a specific metal(loid) in the environment. The  $I_{\text{Geo}}$  values of PM<sub>2.5</sub>-bound metal(loid)s were classified as uncontaminated, uncontaminated to moderately contaminated, moderately contaminated, moderately to heavily contaminated, heavily contaminated, heavily to extremely contaminated and extremely contaminated, when  $I_{\text{Geo}}$  values were less than 0, between 0 and 1, 1 and 2, 2 and 3, 3 and 4, 4 and 5, and greater than 5 [28]. Generally, it may indicate the influence of anthropogenic emissions when  $I_{\text{Geo}}$  values were higher than 1.

### 2.3.3. Population Exposure Assessment Model

#### Population Exposure Dose

Due to long-term exposure to PM<sub>2.5</sub>-bound metal(loid)s in ambient air through ingestion, inhalation, and dermal contact exposure pathways, it may cause potentially adverse population health risks, including non-carcinogenic and carcinogenic risks. A population exposure assessment model was used to evaluate the health risks of PM<sub>2.5</sub>-bound metal(loid)s in ambient air for humans, including children and adults. According to Technical Guideline for Population Exposure Assessment of Environmental Pollutant (HJ 875-2017, [http://www.mee.gov.cn/gkml/hbb/bgg/201711/t20171129\\_427128.htm](http://www.mee.gov.cn/gkml/hbb/bgg/201711/t20171129_427128.htm)), population exposure was defined as average daily population exposure dose (ADPED) of each metal(loid) and was then calculated individually for each metal and exposure pathway, including ingestion (ADPED<sub>Ing</sub>), inhalation (ADPED<sub>Inh</sub>), and dermal contact (ADPED<sub>Der</sub>) as follows:

$$\text{ADPED}_{\text{Ing}} = C_{i_{\text{Aerosol}}} \times \frac{R_{\text{Ing}} \times \text{EF} \times \text{ED}}{\text{BW} \times \text{AT}} \times \text{CF}, \quad (2)$$

$$\text{ADPED}_{\text{Inh}} = C_{i_{\text{Aerosol}}} \times \frac{R_{\text{Inh}} \times \text{EF} \times \text{ED}}{\text{BW} \times \text{AT} \times \text{PEF}}, \quad (3)$$

$$\text{ADPED}_{\text{Der}} = C_{i_{\text{Aerosol}}} \times \frac{\text{SA} \times \text{AF} \times \text{ABS} \times \text{EF} \times \text{ED}}{\text{BW} \times \text{AT}} \times \text{CF}, \quad (4)$$

where  $R_{\text{Ing}}$  and  $R_{\text{Inh}}$  represent the ingestion and inhalation rate, respectively; ABS represents the dermal absorption factor; EF represents the exposure frequency; ED represents the exposure duration; BW represents the body weight; AT represents the averaging time; PEF represents the particle emission factor; SA represents the skin surface area in contact with air; AF represents the adherence factor for fine particulates to skin; CF represents the conversion factor. The Cr concentration was typically equal to the one-seventh of the total Cr concentration because only Cr(VI) was carcinogenic, while Cr(III) was non-carcinogenic [29]. These variables have been described in previous studies [5,30–32] and are listed in Supplementary Table S1.

#### Population Health Carcinogenic and Non-Carcinogenic Risk

The carcinogenic risks (CRs) due to exposure to As, Cd, Co, Cr(VI), Ni, and Pb were equal to ADPED multiplied by a specific slope factor (SF). The non-carcinogenic risks due to exposure to As, Cd, Cr(III), Co, Cu, Mn, Ni, Zn, Pb, Ag, Al, Ba, Mo, Sb, Sr, U, and V were evaluated using the hazard quotient (HQ), which were calculated by dividing ADPED into a specific reference dose (RfD) [29,30,33]. The total carcinogenic risk (TCR) and total hazard index (THI) indicated the mixed carcinogenic and

non-carcinogenic risk due to exposure to an individual metal(loid) and multiple metal(loid)s through three exposure pathways in ambient air, respectively, which were estimated as follows:

$$CR_i = ADED_i \times SF_i, \quad (5)$$

$$HQ_i = \frac{ADED_i}{RfD_i}, \quad (6)$$

$$TCR = \sum CR_i, \quad (7)$$

$$THI = \sum HQ_i, \quad (8)$$

Generally, acceptable CR and TCR values ranging from  $1 \times 10^{-6}$  to  $1 \times 10^{-4}$  suggest that the PM<sub>2.5</sub>-bound metal(loid)s in ambient air does not cause a carcinogenic risk for population health. The carcinogenic risk is categorized as very low, low, moderate, high, and very high for population health when the CR values were less than  $1 \times 10^{-6}$ , between  $1 \times 10^{-6}$  and  $1 \times 10^{-4}$ ,  $1 \times 10^{-4}$  and  $1 \times 10^{-3}$ ,  $1 \times 10^{-3}$  and  $1 \times 10^{-1}$ , and greater than  $1 \times 10^{-1}$  [34]. There was no significant population health non-carcinogenic risk when the HI values were less than 1. Otherwise, there may be non-carcinogenic risks.

### 3. Results and Discussion

#### 3.1. PM<sub>2.5</sub> Mass Concentrations and Pollution Characteristics

Figure 2 presents the time series of mass concentration of PM<sub>2.5</sub>, WSIs, CAs, and TE during 13–23 January 2018 at Xiantao site. There was low atmospheric visibility (2.34 km) for 13–23 January and Xiantao experienced an eleven day-long haze episode with an average daily PM<sub>2.5</sub> mass concentration of  $132 \pm 56.0 \mu\text{g m}^{-3}$ . This level was higher than the levels ( $123 \mu\text{g m}^{-3}$ ) in January from 2012–2017, and approximately 1.76 and 2.49 times higher than the Grade II of NAAQS and the “normal” levels ( $53 \mu\text{g m}^{-3}$ ) without pollution events there in January 2018 (<http://sthjt.hubei.gov.cn/fbjd/zwgk/jcsjfb/hjkq/>), respectively, indicating a heavy PM<sub>2.5</sub> pollution during wintertime in JHP, central China. The average daily WSIs, OC, EC, and TE concentrations were  $83.6 \pm 46.7$ ,  $16.4 \pm 5.75$ ,  $5.56 \pm 1.78$ , and  $7.97 \pm 2.36 \mu\text{g m}^{-3}$ , respectively. The PM<sub>2.5</sub> mass concentrations during severe pollution period ( $277 \pm 20.2 \mu\text{g m}^{-3}$ ) was approximately 2–3 times higher than the levels during mild, moderate, and heavy pollution periods ( $95 \pm 10.5$ ,  $131 \pm 8.52$ , and  $175 \pm 27.3 \mu\text{g m}^{-3}$ , respectively).

When compared to other cities around the world (Table 1), the PM<sub>2.5</sub> concentration in Xiantao was comparable to the level in Tianjin, China ( $124 \mu\text{g m}^{-3}$ ) [11]. The level was much higher compared to most cities in China, including Hefei ( $81.0 \mu\text{g m}^{-3}$ ) [35], Shanghai ( $92.9 \pm 44.4 \mu\text{g m}^{-3}$ ) [14], Huangshi ( $98.3 \mu\text{g m}^{-3}$ ) [36], Nanjing ( $112 \pm 26.4 \mu\text{g m}^{-3}$ ) [13], Chengdu ( $113 \pm 60.3 \mu\text{g m}^{-3}$ ) [15], and Beijing ( $117 \mu\text{g m}^{-3}$ ) [11], and in other countries, such as Iasi (Romania,  $23.4 \pm 11.7 \mu\text{g m}^{-3}$ ) [37], Zonguldak (Turkey,  $37.3 \mu\text{g m}^{-3}$ ) [38], and Riyadh (Saudi Arabia,  $71.9 \mu\text{g m}^{-3}$ ) [39]. The level was significantly lower compared to some cities in China, such as Guilin ( $144 \pm 28.5 \mu\text{g m}^{-3}$ ) [40], Wuhan ( $160 \pm 66.3 \mu\text{g m}^{-3}$ ) [17], Xiangyang ( $169 \pm 57.0 \mu\text{g m}^{-3}$ ) [18], Zhengzhou ( $188 \pm 52.4 \mu\text{g m}^{-3}$ ) [16], Shijiazhuang ( $234 \pm 140 \mu\text{g m}^{-3}$ ) [12], and Xi’an ( $537 \pm 146 \mu\text{g m}^{-3}$ ) [10], and in other developing countries, such as Delhi (India,  $293 \pm 36.7 \mu\text{g m}^{-3}$ ) [41].

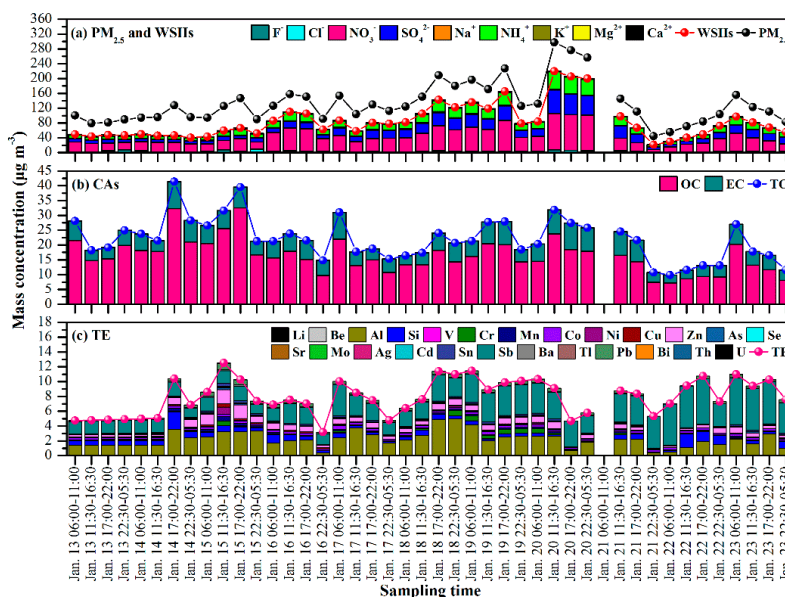


**Figure 2.** Time series of mass concentration of (a) PM<sub>2.5</sub> and WSIs, (b) CAs, and (c) TE during 13–23 January 2018 at Xiantao site.

**Table 1.** Reported PM<sub>2.5</sub> mass concentrations (Mean ± Standard deviation, µg m<sup>-3</sup>) in Xiantao compared to other cities around the world.

Station (Country)	Site Type	Field Sampling Campaign	Mean ± Standard Deviation	References
Xiantao (China)	Urban	13–23 January 2018	132 ± 56.0	This Study
Zonguldak (Turkey)	Urban	Winter, 2007	37.3	[38]
Xi’an (China)	Urban	17–26 December 2013	537 ± 146	[10]
Riyadh (Saudi Arabia)	Urban	January 2013	71.9	[39]
Wuhan (China)	Urban	9 January 2013–6 February 2013	160 ± 66.3	[17]
Delhi (India)	Near-road	December 2013–January 2014	293 ± 36.7	[41]
Nanjing (China)	Urban	Winter, 2014	112 ± 26.4	[13]
Beijing (China)	Urban	29 December 2014–27 January 2015	117	[11]
Tianjin (China)	Urban	2015	124	[11]
Iasi (Romania)	Urban	January 2016	23.4 ± 11.7	[37]
Shijiazhuang (China)	Urban	15 December 2015–14 January 2016	234 ± 140	[12]
Hefei (China)	Industrial	October 2016–January 2017	81.0	[35]
Guilin (China)	Urban	10–15 December 2016–4–7 January 2017	144 ± 28.5	[40]
Shanghai (China)	Suburban	2018 haze days	92.9 ± 44.4	[14]
Chengdu (China)	Near-road	Winter, 2018	113 ± 60.3	[15]
Huangshi (China)	Industrial	13–25 January 2018	98.3	[36]
Zhengzhou (China)	Urban	11–23 January 2018	188 ± 52.4	[16]
Xiangyang (China)	Urban	13–24 January 2018	169 ± 57.0	[18]

The PM<sub>2.5</sub> concentration reached the highest value on 20 January during severe pollution period. The phenomenon could have been caused by the air masses from the WNW-NNE direction (first comes from the WNW direction and then turn around from the NNE direction to approach the Xiantao site), accounting for 50% of all the trajectories (Figure 3), which could be found by the highest average concentrations of PM<sub>2.5</sub> (153 ± 69.5 µg m<sup>-3</sup>) and WSIs (104 ± 55.6 µg m<sup>-3</sup>) (Supplementary Table S2). These air-masses originated from Xiangyang, passed through Suizhou, Xiaogan and Wuhan, and then approached the Xiantao site with a much lower transport speed during severe pollution period (Supplementary Figure S1), which was not conducive to the horizontal transport for ambient air pollutants. In contrast, the PM<sub>2.5</sub> concentration reached the lowest value on 21 January during mild

pollution period. This phenomenon could have been partially caused by the air masses from the NE direction, accounting for 7% of all the trajectories (Figure 3), which could be found by the lowest average concentration of PM<sub>2.5</sub> ( $96.7 \pm 19.8 \mu\text{g m}^{-3}$ ) (Supplementary Table S2). These air-masses initiated in Anhui Province, then passed through Jiangsu province, and finally entered Hubei Province to approach Xiantao site with a higher transport speed during mild pollution period, which was conducive to the horizontal transport for ambient air pollutants. In addition, rainy and snowy weather (0.30 mm prec.) was observed from midnight of 20 January until the afternoon of 21 January, and thus significantly reduced the PM<sub>2.5</sub> concentration through the wet deposition (Supplementary Figure S1).

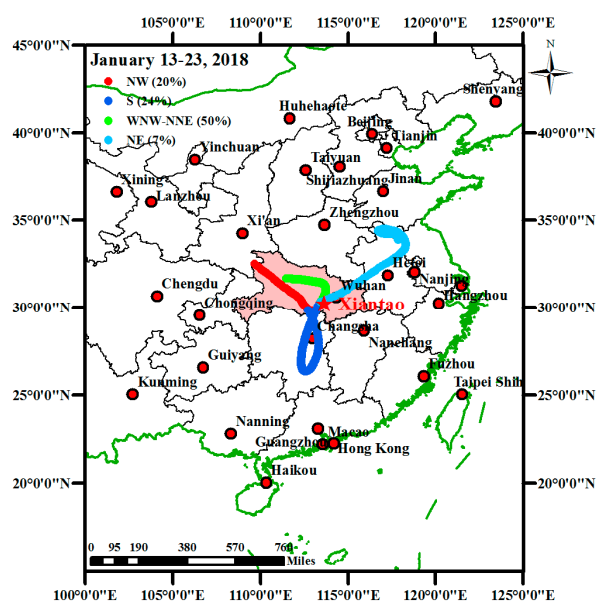


**Figure 3.** Four simulated clusters for 3 days (72 h) air masses back trajectories every four times a day at 500 m A.G.L using HYSPLIT model (<https://www.arl.noaa.gov/hysplit/>) during 13–23 January 2018 at Xiantao site.

### 3.2. Chemical Compositions

#### 3.2.1. WSIs

Figure 4a presents the WSIs concentration, Secondary inorganic aerosol (SNA, including  $\text{SO}_4^{2-}$ ,  $\text{NO}_3^-$ , and  $\text{NH}_4^+$ )/WSIs and WSIs/PM<sub>2.5</sub> ratios at different pollution levels. SNA accounted for  $91.4 \pm 4.89\%$  of total WSIs, ranging from 76.9% to 96.3%. The average WSIs/PM<sub>2.5</sub> ratios were  $60.8 \pm 9.82\%$ , indicating that WSIs accounted for the most percentage of PM<sub>2.5</sub> mass concentration. It should be noted that the WSIs concentration increased as the pollution levels increased: mild pollution ( $54.7 \pm 11.0 \mu\text{g m}^{-3}$ ) < moderate pollution ( $76.3 \pm 14.7 \mu\text{g m}^{-3}$ ) < heavy pollution ( $119 \pm 23.5 \mu\text{g m}^{-3}$ ) < severe pollution ( $208 \pm 10.1 \mu\text{g m}^{-3}$ ). Moreover, the SNA/WSIs and WSIs/PM<sub>2.5</sub> ratios increased as pollution levels increased, which indicated the intensification of secondary formation during the winter haze episode in Xiantao, consistent with our previous simultaneously field sampling campaign conducted in Xiangyang [18].

The acidity of PM<sub>2.5</sub> (Supplementary Text S1) could be roughly evaluated through the balance of anions and cations [42]. The average anions/cations ratios during mild, moderate, heavy, and severe pollution periods were  $1.04 \pm 0.06$ ,  $1.00 \pm 0.09$ ,  $1.05 \pm 0.02$ , and  $1.09 \pm 0.03$ , respectively. All these ratios approached 1 and strong positive correlations ( $r = 0.93, 0.86, 0.99, \text{ and } 0.82$ , respectively,  $p < 0.05$ ) between anions and cations were observed at different pollution levels in Xiantao (Figure 4b), which indicated that almost all the WSIs were identified and these WSIs were important alkaline and acidic species in the PM<sub>2.5</sub> aerosol [43]. Moreover, all these ratios were also greater than 1, which may be due to a deficiency of  $\text{H}^+$  in the calculation and/or to  $\text{NH}_4^+$  being converted into the

gaseous phase [22]. The anions/cations ratios is also a good indicator for studying the acidity of PM<sub>2.5</sub> aerosols [22], which indicated that the PM<sub>2.5</sub> aerosols were acidic during the winter haze episode in Xiantao.

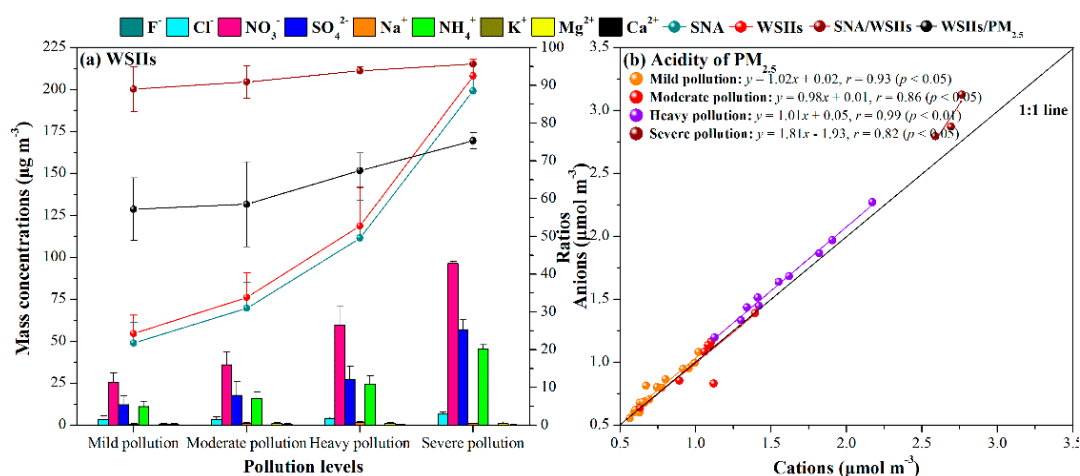


**Figure 4.** Dynamic variations of (a) WSIs, SNA/WSIs and WSIs/PM<sub>2.5</sub> ratios, and (b) acidity of PM<sub>2.5</sub> at different pollution levels at Xiantao site.

The  $\text{NO}_3^-/\text{SO}_4^{2-}$  ratio has been generally used as an indicator to evaluate the relative contribution of local stationary sources (e.g., coal-fired power plant) and local mobile sources (e.g., vehicle exhaust) to sulfur and nitrogen in the ambient air [44,45]. In this study, the average  $\text{NO}_3^-/\text{SO}_4^{2-}$  ratios during mild, moderate, heavy, and severe pollution periods were  $2.35 \pm 0.78$ ,  $2.39 \pm 1.08$ ,  $2.31 \pm 0.62$ , and  $1.70 \pm 0.15$ , respectively, which indicated that local mobile sources contributed more to PM<sub>2.5</sub> compared to local stationary sources during the winter haze episode. Generally, the sulfur oxidation ratio (SOR) and nitrogen oxidation ratio (NOR) values (Supplementary Text S1) were less than 0.10 for primary pollutants, whereas they were greater than 0.10 when gaseous precursors ( $\text{SO}_2$  and  $\text{NO}_2$ ) were photochemically oxidized in the ambient air [46,47]. The SOR and NOR values during mild, moderate, heavy, and severe pollution periods were  $0.38 \pm 0.25$  and  $0.28 \pm 0.09$ ,  $0.45 \pm 0.27$  and  $0.30 \pm 0.09$ ,  $0.65 \pm 0.11$  and  $0.47 \pm 0.05$ , and  $0.66 \pm 0.04$  and  $0.47 \pm 0.05$ , respectively (Supplementary Figure S2), which indicated that the significantly secondary transformations of  $\text{SO}_2$  to  $\text{SO}_4^{2-}$  and  $\text{NO}_2$  to  $\text{NO}_3^-$  were observed during the winter haze episode.

### 3.2.2. CAs

The average OC and EC concentrations during the winter haze episode were  $16.4 \pm 5.74$  and  $5.56 \pm 1.78 \mu\text{g m}^{-3}$ , respectively, which accounted for  $74.3 \pm 4.60\%$  and  $25.7 \pm 4.60\%$  of TC. The OC, EC, and TC concentrations basically increased as the pollution levels increased, except for OC and TC during heavy pollution period. The OC concentration reached the maximum and minimum values at 17:00–22:00 on 15 January ( $32.5 \mu\text{g m}^{-3}$ ) during the moderate pollution period and at 06:00–11:00 on 22 January ( $7.21 \mu\text{g m}^{-3}$ ) during mild pollution period, respectively. The EC concentration reached the maximum and minimum values at 17:00–22:00 on 14 January ( $9.05 \mu\text{g m}^{-3}$ ) during moderate pollution period and at 06:00–11:00 on 22 January ( $2.66 \mu\text{g m}^{-3}$ ) during mild pollution period, respectively. In addition, the OC/EC ratios ranged from 1.89 to 4.83 with an average OC/EC ratio of  $3.01 \pm 0.76$ .

The OC/EC ratios increased as the pollution levels increased from mild to moderate pollution, whereas the ratios decreased as the pollution levels increased from moderate to severe pollution, thus reached the highest levels during moderate pollution period (Figure 5, which indicated that more SOA were formed during moderate pollution period compared to the other three pollution levels. Moreover, the average OC/EC ratios at four pollution levels ( $3.06 \pm 0.85$ ,  $3.42 \pm 0.87$ ,  $2.81 \pm 0.39$ , and  $2.42 \pm 0.46$ , respectively) were higher than 2, indicating that secondary organic aerosol (SOA) were

formed during the winter haze episode. OC was positively correlated with EC ( $r = 0.71, p < 0.05$ ), which indicated that there may be a certain same emission source during the winter haze episode. 32.6% of OC/EC ratios ranged from 1.5 to 2.5 ( $r = 0.95, p < 0.05$ ) (Supplementary Figure S3), it may indicate the contribution of intensive vehicle exhaust to CAs, whereas 67.4% of the OC/EC ratios were higher than 2.5 ( $r = 0.83, p < 0.05$ ), which might suggest a rapid transformation of secondary organic carbon (SOC) precursors such as VOCs [48].

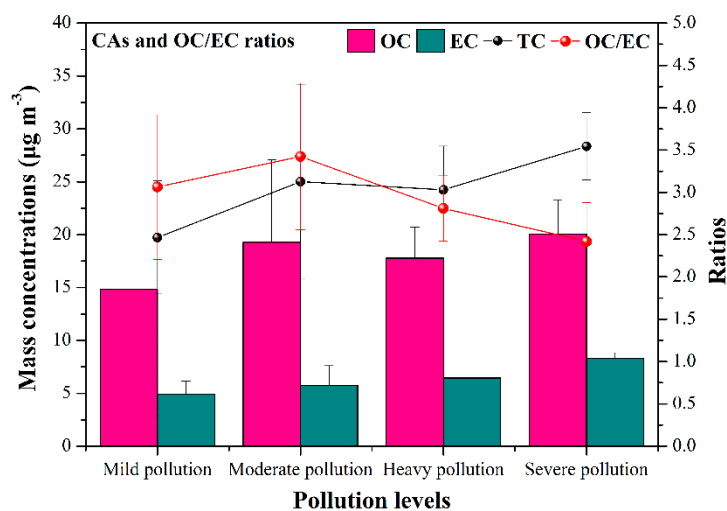


**Figure 5.** Dynamic variations of CAs (OC, EC, and TC) and OC/EC ratios at different pollution levels at Xiantao site.

### 3.2.3. TE

The TE concentrations during mild, moderate, heavy, and severe pollution periods were  $6.64 \pm 2.18$ ,  $9.26 \pm 1.89$ ,  $9.59 \pm 1.70$ , and  $6.52 \pm 2.30 \mu\text{g m}^{-3}$ , respectively. The proportion of TE to  $\text{PM}_{2.5}$  was  $6.04 \pm 1.79\%$ . The sum of Sb, Al, Si, Zn, Pb, Co, Cr, Mn, Sn, and Cu concentrations accounted for 95.7% of total TE. Figure S4a shows the dynamic variations of TE mass concentrations at the four ambient air quality levels. The Si, Mn, Ni, Cu, Zn, As, Se, Sr, Ag, Cd, Sn, Ba, Pb, and Bi concentrations increased as the pollution levels increased from mild to moderate pollution, whereas these concentrations decreased as the pollution levels from moderate to severe pollution. The Al, Cr, Co, and Sb concentrations increased as the pollution levels increased from mild to heavy pollution, whereas these concentrations decreased as the pollution levels from heavy to severe pollution. The other TE concentrations fluctuated at four pollution levels. The average TE concentration reached the higher value during 18 January to 23 January. The phenomenon could have been partially caused by the air masses from the NE and WNW-NNE directions, accounting for 7% ( $8.93 \pm 1.91 \mu\text{g m}^{-3}$ ) and 50% ( $8.54 \pm 2.31 \mu\text{g m}^{-3}$ ) of all the trajectories (Figure 3 and Supplementary Table S2), respectively. The former air-masses originated from Anhui Province, passed through Shandong Province, and then turn around to approach the Xiantao site with a much higher transport speed during mild pollution period (Supplementary Figure S1) due to long-range transport, which may carry lots of ambient air pollutants to the region. The latter air-masses originated from Xiangyang, passed through Suizhou, Xiaogan, and Wuhan, and then approached the Xiantao site with a much lower transport speed due to combined effect of long-range transport and local emissions (Supplementary Figure S1). Moreover, the rains and snowy weather occurred in the evening of 23 January may increase the hygroscopic growth. In contrast, the average TE concentration reached the lower value during 13 January to 17 January. This phenomenon could have been partially caused by the air masses from the S and NW directions, accounting for 24% ( $7.59 \pm 2.76 \mu\text{g m}^{-3}$ ) and 20% ( $6.68 \pm 2.10 \mu\text{g m}^{-3}$ ) of all the trajectories (Figure 3 and Supplementary Table S2). The former air-masses initiated in Shiyan, then passed through Jingmen, and finally approached the Xiantao site with a lower transport speed (Supplementary Figure S1).

The latter air masses originated from Xiantao, passed through Yueyang and Changsha, and then turn around to approach the Xiantao site with a much higher transport speed (Supplementary Figure S1). Both may be due to the combined effect of long-range transport and local emissions.

The Pb/Cd ratio is generally considered as an indicator to identify the sources of TE [49]. In our study, the Pb/Cd ratios during mild, moderate, heavy, and severe pollution periods were  $35.9 \pm 33.7$ ,  $34.7 \pm 9.14$ ,  $40.5 \pm 7.94$ , and  $44.4 \pm 2.89$ , respectively. These ratios were close to the ratios for anthropogenic emissions (46), indicating that Pb and Cd may be emitted from anthropogenic emissions. Moreover, the V/Ni ratio is commonly used to distinguish industrial emissions (0.7–1.9) and shipping emissions (2.1–3.1) [49,50]. The V/Ni ratios were found to be within the range of 0.7–1.9 during mild and severe pollution periods (1.80 and 1.59, respectively), which indicated that V and Ni may come from industrial emissions during these two periods. This might be mainly affected by the air masses from the NE and WNW-NNE directions due to combined effect of long-range transport and local emissions as mentioned above. In addition, Pb was positively correlated with Cd ( $r = 0.96$ ,  $p < 0.05$ ) during the moderate pollution period, which indicated that the Pb and Cd may have same emission sources during this period. Similar results for V and Ni ( $r = 0.69$ ,  $p < 0.05$ ) were observed during heavy pollution period.

Figure 6a and Supplementary Figure S5 present EF and  $I_{Geo}$  values for PM<sub>2.5</sub>-bound metal(loid)s at different pollution levels. Except for Al and Th, the average EF values (Supplementary Text S2) for PM<sub>2.5</sub>-bound metal(loid)s widely ranged from 3 to 90,717 during the winter haze episode in Xiantao (Figure 6a), which indicated that PM<sub>2.5</sub>-bound metal(loid)s were affected by natural and anthropogenic activities. The EF values of U, Ba, Sr, Mn, Li, and V were within the range of 2–10, which suggested that these metal(loid)s were mixed affected by crustal sources and anthropogenic emissions. In contrast, the EF values of most metal(loid)s, including Be, Cr, Ni, Cu, Mo, Tl, Zn, Ag, As, Pb, Co, Bi, Cd, Sn, Se, and Sb were significantly higher than 10, indicating the predominate influence from anthropogenic emissions on these metal(loid)s (Supplementary Figure S5). As shown in Figure 6a, the  $I_{Geo}$  values of Li, Al, Th, U, Ba, Sr, V, and Mn were lower than 0, indicating that these metal(loid)s were uncontaminated. The  $I_{Geo}$  values of Be ranged from 1 to 2, which indicated that there was moderate contamination for Be. The metals of Cr and Ni were moderately to heavily contaminated because the  $I_{Geo}$  values of them ranged from 2 to 3. Mo was heavily contaminated because the  $I_{Geo}$  values ranged from 3 to 4. Cu and Tl were heavily to extremely contaminated because the  $I_{Geo}$  values of them ranged from 4 to 5. What calls for special attention is the extreme contamination for Zn, As, Ag, Pb, Co, Bi, Cd, Sn, Se, and Sb because the  $I_{Geo}$  values of these metals were higher than 5, which may have caused population health carcinogenic or non-carcinogenic risk to some extent. It should be noted that EF values were positively correlated with  $I_{Geo}$  values at the four pollution levels ( $r = 0.99$ ,  $p < 0.01$ ) (Supplementary Figure S4b), which indicated that the dynamic variation trends of EF and  $I_{Geo}$  values remained consistent during the winter haze episode.

### 3.3. Chemical Mass Closure

The chemical mass closure method (Supplementary Text S3) was used to better understand PM<sub>2.5</sub> chemical compositions, including mineral dust (MD), trace element oxides (TEO), OM, EC, SNA, Cl<sup>−</sup> and unidentified matters (UM) [51–53]. Figure 7a–e presents the chemical mass closure for PM<sub>2.5</sub> at different pollution levels at Xiantao site. As shown in Figure 7a, SNA occupied the largest proportion (58.6%) of PM<sub>2.5</sub>, followed by OM (19.9%), MD (4.31%), EC (4.21%), TEO (4.21%), and Cl<sup>−</sup> (2.76%). The contributions of MD, TEO, OM, EC, and Cl<sup>−</sup> to PM<sub>2.5</sub> decreased as the pollution levels increased, whereas the contribution of SNA to PM<sub>2.5</sub> increased as pollution levels increased (Figure 7b–e). The results may indicate the contribution variations of emission sources to PM<sub>2.5</sub> chemical compositions. On average, only a small proportion of PM<sub>2.5</sub> (UM, 6.02%) cannot be identified in this study as well as each pollution level, which indicated that the chemical masses of PM<sub>2.5</sub> aerosol samples were balanced during the winter haze episode in Xiantao.

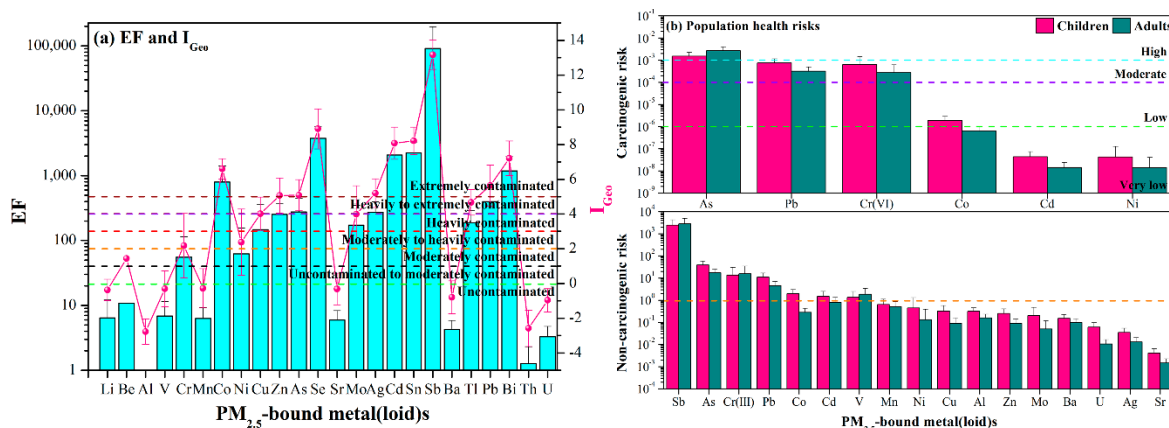


Figure 6. The (a) EF and I<sub>Geo</sub>, and (b) population health risks for PM<sub>2.5</sub>-bound metal(loids) during the winter haze episode.

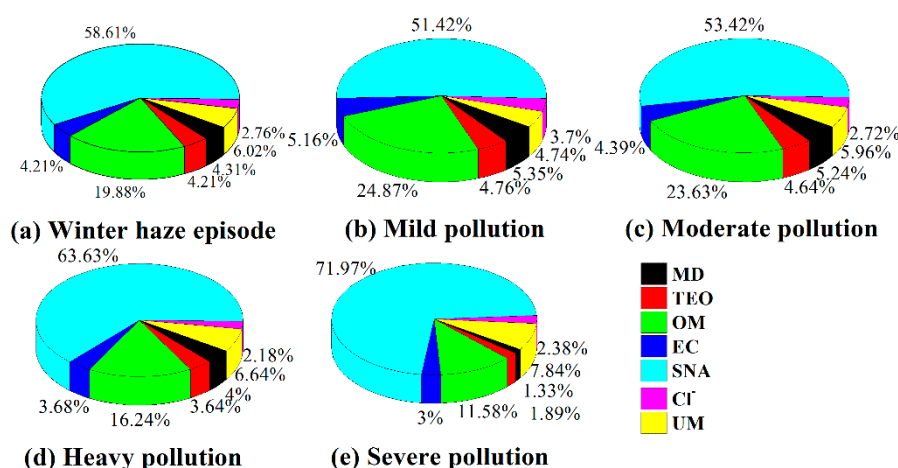


Figure 7. Chemical mass closure for PM<sub>2.5</sub> at Xiantao site at different pollution levels: (a) winter haze episode, (b) mild pollution, (c) moderate pollution, (d) heavy pollution, and (e) severe pollution.

### 3.4. Population Exposure Assessment

#### 3.4.1. Population Exposure Dose

Table 2 presents ADPED values of PM<sub>2.5</sub>-bound metal(loids) through ingestion, inhalation, and dermal contact pathways for children and adults during the winter haze episode. Sb showed the maximum ADPED values of PM<sub>2.5</sub>-bound metal(loids) through these three different exposure pathways for children ( $3.66 \times 10^{-1}$ ) and adults ( $5.96 \times 10^{-2}$ ), whereas U showed the minimum ADPED values of PM<sub>2.5</sub>-bound metal(loids) through these three different exposure pathways for children ( $3.64 \times 10^{-5}$ ) and adults ( $5.92 \times 10^{-6}$ ), respectively. Ingestion is found to be the dominant exposure pathway of PM<sub>2.5</sub>-bound metal(loids) for children and adults in Xiantao, followed by inhalation and dermal contact, which agreed with previous studies in Kanpur, India [54] and Xiangyang, central China [18]. As shown in Supplementary Table S3, the ADPED values of PM<sub>2.5</sub>-bound metal(loids) through ingestion pathway were 1–4 orders of magnitude higher for children and adults at the four pollution levels compared to inhalation and dermal contact pathways. It should be noted that ADPED values of PM<sub>2.5</sub>-bound metal(loids) through these three exposure pathways for children were 5.74-fold higher than the values for adults, which indicated that children were more likely to be exposed to PM<sub>2.5</sub>-bound metal(loids) than adults during the winter haze episode in Xiantao.

**Table 2.** The ADPED ( $\text{mg kg}^{-1} \text{ day}^{-1}$ ) of  $\text{PM}_{2.5}$ -bound metal(loid)s through ingestion, inhalation, and dermal contact pathways for children and adults during the winter haze episode.

PM <sub>2.5</sub> -Bound Metal(loid)s	Children			Adults				
	ADPED <sub>Ing</sub> *	ADPED <sub>Inh</sub> *	ADPED <sub>Der</sub> *	ADPED	ADPED <sub>Ing</sub> *	ADPED <sub>Inh</sub> *	ADPED <sub>Der</sub> *	ADPED
Sb	$3.54 \times 10^{-1}$	$2.60 \times 10^{-5}$	$1.24 \times 10^{-2}$	$3.66 \times 10^{-1}$	$3.79 \times 10^{-2}$	$2.12 \times 10^{-6}$	$2.16 \times 10^{-2}$	$5.96 \times 10^{-2}$
Al	$2.24 \times 10^{-1}$	$1.65 \times 10^{-5}$	$7.85 \times 10^{-3}$	$2.32 \times 10^{-1}$	$2.40 \times 10^{-2}$	$1.34 \times 10^{-6}$	$1.37 \times 10^{-2}$	$3.78 \times 10^{-2}$
Zn	$6.45 \times 10^{-2}$	$4.74 \times 10^{-6}$	$2.26 \times 10^{-3}$	$6.67 \times 10^{-2}$	$2.29 \times 10^{-3}$	$1.28 \times 10^{-7}$	$1.30 \times 10^{-3}$	$3.59 \times 10^{-3}$
Pb	$3.35 \times 10^{-2}$	$2.46 \times 10^{-6}$	$1.17 \times 10^{-3}$	$3.47 \times 10^{-2}$	$4.44 \times 10^{-3}$	$2.48 \times 10^{-7}$	$2.53 \times 10^{-3}$	$6.97 \times 10^{-3}$
Co	$3.22 \times 10^{-2}$	$2.37 \times 10^{-6}$	$1.13 \times 10^{-3}$	$3.33 \times 10^{-2}$	$3.86 \times 10^{-3}$	$2.15 \times 10^{-7}$	$2.20 \times 10^{-3}$	$6.05 \times 10^{-3}$
Cr	$1.74 \times 10^{-2}$	$1.28 \times 10^{-6}$	$6.09 \times 10^{-4}$	$1.80 \times 10^{-2}$	$2.72 \times 10^{-3}$	$1.52 \times 10^{-7}$	$1.55 \times 10^{-3}$	$4.27 \times 10^{-3}$
Mn	$1.41 \times 10^{-2}$	$1.03 \times 10^{-6}$	$4.92 \times 10^{-4}$	$1.46 \times 10^{-2}$	$1.51 \times 10^{-3}$	$8.42 \times 10^{-8}$	$8.59 \times 10^{-4}$	$2.36 \times 10^{-3}$
Cu	$1.16 \times 10^{-2}$	$8.53 \times 10^{-7}$	$4.06 \times 10^{-4}$	$1.20 \times 10^{-2}$	$1.24 \times 10^{-3}$	$6.95 \times 10^{-8}$	$7.09 \times 10^{-4}$	$1.95 \times 10^{-3}$
As	$1.00 \times 10^{-2}$	$7.38 \times 10^{-7}$	$1.05 \times 10^{-3}$	$1.11 \times 10^{-2}$	$1.33 \times 10^{-3}$	$7.43 \times 10^{-8}$	$2.27 \times 10^{-3}$	$3.60 \times 10^{-3}$
Ni	$8.66 \times 10^{-3}$	$6.37 \times 10^{-7}$	$3.03 \times 10^{-4}$	$8.96 \times 10^{-3}$	$1.15 \times 10^{-3}$	$6.41 \times 10^{-8}$	$6.54 \times 10^{-4}$	$1.80 \times 10^{-3}$
Ba	$6.95 \times 10^{-3}$	$5.11 \times 10^{-7}$	$2.43 \times 10^{-4}$	$7.20 \times 10^{-3}$	$3.03 \times 10^{-4}$	$1.69 \times 10^{-8}$	$1.72 \times 10^{-4}$	$4.75 \times 10^{-4}$
Sr	$2.11 \times 10^{-3}$	$1.55 \times 10^{-7}$	$7.38 \times 10^{-5}$	$2.18 \times 10^{-3}$	$2.26 \times 10^{-4}$	$1.26 \times 10^{-8}$	$1.29 \times 10^{-4}$	$3.55 \times 10^{-4}$
V	$2.08 \times 10^{-3}$	$1.53 \times 10^{-7}$	$7.29 \times 10^{-5}$	$2.16 \times 10^{-3}$	$2.23 \times 10^{-4}$	$1.25 \times 10^{-8}$	$1.27 \times 10^{-4}$	$3.51 \times 10^{-4}$
Cd	$1.19 \times 10^{-3}$	$8.75 \times 10^{-8}$	$4.17 \times 10^{-6}$	$1.19 \times 10^{-3}$	$1.58 \times 10^{-4}$	$8.82 \times 10^{-9}$	$8.99 \times 10^{-6}$	$1.67 \times 10^{-4}$
Mo	$9.30 \times 10^{-4}$	$6.84 \times 10^{-8}$	$3.26 \times 10^{-5}$	$9.63 \times 10^{-4}$	$9.97 \times 10^{-5}$	$5.57 \times 10^{-9}$	$5.68 \times 10^{-5}$	$1.56 \times 10^{-4}$
Ag	$1.47 \times 10^{-4}$	$1.08 \times 10^{-8}$	$5.13 \times 10^{-6}$	$1.52 \times 10^{-4}$	$1.57 \times 10^{-5}$	$8.78 \times 10^{-10}$	$8.96 \times 10^{-6}$	$2.47 \times 10^{-5}$
U	$3.52 \times 10^{-5}$	$2.59 \times 10^{-9}$	$1.23 \times 10^{-6}$	$3.64 \times 10^{-5}$	$3.77 \times 10^{-6}$	$2.11 \times 10^{-10}$	$2.15 \times 10^{-6}$	$5.92 \times 10^{-6}$

\* ADPED<sub>Ing</sub>, ADPED<sub>Inh</sub>, and ADPED<sub>Der</sub> represent the average daily population exposure dose due to exposure to  $\text{PM}_{2.5}$ -bound metal(loid)s through ingestion, inhalation, and dermal contact pathways, respectively.

### 3.4.2. Population Health Risks

Figure 6b and Supplementary Figure S6a–d presents the population health carcinogenic risk and non-carcinogenic risk due to personal exposure to PM<sub>2.5</sub>-bound metal(loid)s at different pollution levels for children and adults, respectively. The highest carcinogenic risk for children and adults during the winter haze episode was As ( $1.49 \times 10^{-3}$  and  $2.59 \times 10^{-3}$ ), followed by Pb ( $7.40 \times 10^{-4}$  and  $3.17 \times 10^{-4}$ ), Cr(VI) ( $6.37 \times 10^{-4}$  and  $2.72 \times 10^{-4}$ ), Co ( $1.91 \times 10^{-6}$  and  $6.22 \times 10^{-7}$ ), Cd ( $4.35 \times 10^{-8}$  and  $1.42 \times 10^{-8}$ ), and Ni ( $4.22 \times 10^{-8}$  and  $1.37 \times 10^{-8}$ ). The CR values through ingestion, inhalation, and dermal contact exposure pathways widely ranged from  $4.22 \times 10^{-8}$  to  $1.49 \times 10^{-3}$  for children and  $1.37 \times 10^{-8}$  to  $2.59 \times 10^{-3}$  for adults. Moreover, the TCR values were approximately 1.12-fold higher for adults ( $3.22 \times 10^{-3}$ ) than for children ( $2.87 \times 10^{-3}$ ), which indicated that PM<sub>2.5</sub>-bound metal(loid)s may pose much higher carcinogenic risk for adults compared to children during the winter haze episode in Xiantao (Figure 6b). The CRs value for As is 1~5 orders of magnitude higher than the values for other PM<sub>2.5</sub>-bound metal(loid)s for children and adults. The TCR value is the sum of CR values for As, Cd, Co, Cr(VI), Ni, and Pb, which mainly depended on the CR value for As. The CR value for As for children ( $1.49 \times 10^{-3}$ ) is lower than the value for adults ( $2.63 \times 10^{-3}$ ), although the CR values for other PM<sub>2.5</sub>-bound metal(loid)s for children were higher than the values for adults. Therefore, the TCR values were approximately 1.12-fold higher for adults than for children. The TCR values through the three exposure pathways for children and adults during moderate pollution period ( $1.86 \times 10^{-3}$  and  $3.28 \times 10^{-3}$ ) were the highest, followed by mild pollution ( $1.55 \times 10^{-3}$  and  $2.73 \times 10^{-3}$ ), heavy pollution ( $1.20 \times 10^{-3}$  and  $2.11 \times 10^{-3}$ ), and severe pollution periods ( $3.62 \times 10^{-4}$  and  $6.38 \times 10^{-4}$ ) (Supplementary Figure S6a–d). The TCR values through the three exposure pathways for children and adults in Xiantao were lower than the values during the four pollution periods (mild pollution:  $1.64 \times 10^{-1}$ ,  $2.21 \times 10^{-1}$ ; moderate pollution:  $2.71 \times 10^{-3}$ ,  $3.77 \times 10^{-3}$ ; heavy pollution:  $2.27 \times 10^{-3}$ ,  $2.30 \times 10^{-3}$ ; severe pollution:  $1.48 \times 10^{-3}$ ,  $1.65 \times 10^{-3}$ ) in Xiangyang [18]. Among all the PM<sub>2.5</sub>-bound metal(loid)s, the TCR of As, Cr(VI), and Pb for children and adults were at the moderate or high levels, whereas the TCR of Cd, Ni and Co for children and adults were below moderate levels, except for the low carcinogenic risk level of Co for children.

The highest non-carcinogenic risk during the winter haze episode for children and adults was Sb ( $2.43 \times 10^3$  and  $2.80 \times 10^3$ ), followed by As (38.7 and 17.1), Cr(III) (13.6 and 15.6), Pb (10.9 and 4.54), and V (1.34 and 1.85). In addition, Co (2.01) and Cd (1.48) may only pose non-carcinogenic risks for children during the winter haze episode. The HQ values through the three exposure pathways widely ranged from  $4.13 \times 10^{-3}$  to  $2.43 \times 10^3$  for children and  $1.45 \times 10^{-3}$  to  $2.80 \times 10^3$  for adults. Moreover, the THI values were approximately 1.14-fold higher for adults ( $2.84 \times 10^3$ ) than for children ( $2.50 \times 10^3$ ), which indicated that PM<sub>2.5</sub>-bound metal(loid)s may pose much higher non-carcinogenic risk for adults compared to children during the winter haze episode in Xiantao (Figure 6b). The THI values through the three exposure pathways for children and adults decreased as pollution levels increased: mild pollution ( $2.42 \times 10^3$  and  $2.74 \times 10^3$ ) > moderate pollution period ( $2.07 \times 10^3$  and  $2.32 \times 10^3$ ) > heavy pollution ( $1.87 \times 10^3$  and  $2.12 \times 10^3$ ) > severe pollution ( $1.13 \times 10^3$  and  $1.29 \times 10^3$ ) (Supplementary Figure S6a–d). The THI values through the three exposure pathways for children and adults in Xiantao were lower than the values during mild ( $4.22 \times 10^3$ ,  $4.84 \times 10^3$ ) and moderate ( $2.49 \times 10^3$ ,  $2.81 \times 10^3$ ) pollution periods in Xiangyang, whereas the THI values for children and adults were higher than the values during heavy ( $1.65 \times 10^3$ ,  $1.86 \times 10^3$ ) and severe ( $1.05 \times 10^3$ ,  $1.19 \times 10^3$ ) pollution periods in Xiangyang [18]. The total non-carcinogenic risk of Sb for children and adults through the three exposure pathways were 3–6 orders of magnitude higher at the four pollution levels compared to other PM<sub>2.5</sub>-bound metal(loid)s. It should be noted that As, Cr, and Pb may pose carcinogenic and non-carcinogenic risks for children and adults, whereas Sb and V may only pose non-carcinogenic risks for children and adults. Moreover, the population health risks of PM<sub>2.5</sub>-bound metal(loid)s may not depend on the pollution levels but depend on the PM<sub>2.5</sub>-bound metal(loid)s concentrations. Other CAs, such as polycyclic aromatic hydrocarbons (PAHs) could also pose population health risks and needed to be addressed in the future. The government and the public

should pay more attention to the population health risks posed by PM<sub>2.5</sub>-bound metal(loid)s during the winter haze episode in JHP, central China.

#### 4. Conclusions

In this study, a total of 43 pairs of PM<sub>2.5</sub> samples were effectively collected to determine the pollution characteristics, chemical compositions, and population health risks during 13–23 January 2018 in Xiantao in JHP, central China. During the sampling period, Xiantao experienced an eleven-day long-lasting haze episode with an average daily PM<sub>2.5</sub> mass concentration of  $132 \pm 56.0 \mu\text{g m}^{-3}$ . The level was higher than the levels ( $123 \mu\text{g m}^{-3}$ ) in January from 2012 to 2017, and approximately 1.76 and 2.49 times than the Grade II of NAAQS the “normal” levels ( $53 \mu\text{g m}^{-3}$ ) without pollution events there in January 2018, respectively, indicating a heavy PM<sub>2.5</sub> pollution during wintertime in JHP, central China. The PM<sub>2.5</sub> typical chemical compositions for the average WSIs, OC, EC, and TE concentrations were  $83.6 \pm 46.7$ ,  $16.4 \pm 5.75$ ,  $5.56 \pm 1.78$ , and  $7.97 \pm 2.36 \mu\text{g m}^{-3}$ , respectively. The higher PM<sub>2.5</sub> levels during severe pollution period were dominated by the air masses from the WNW-NNE direction, whereas the lower PM<sub>2.5</sub> concentrations during other pollution periods were mainly affected by the air masses from the NE, S, and NW directions.

The anions/cations ratios indicated that the PM<sub>2.5</sub> aerosols were acidic during the winter haze episode in Xiantao. The  $\text{NO}_3^-/\text{SO}_4^{2-}$  ratio indicated that the mobile sources contributed more to PM<sub>2.5</sub> compared to the stationary sources. The OC/EC ratios indicated a mixed contribution of intensive vehicle exhaust and secondary formations. The Pb/Cd and ratios indicated that Pb and Cd may be emitted from anthropogenic emissions. The V/Ni ratios indicated that V and Ni may come from the industrial emissions during mild and severe pollution periods. The EF values were positively correlated with the  $I_{\text{Geo}}$  values at the four pollution levels. Ingestion is found to be the dominant exposure pathway of PM<sub>2.5</sub>-bound metal(loid)s for children and adults in Xiantao, followed by inhalation and dermal contact. As, Cr, and Pb may pose carcinogenic and non-carcinogenic risks for children and adults, whereas Sb and V may only pose non-carcinogenic risks for children and adults. PM<sub>2.5</sub>-bound metal(loid)s may pose much higher population health risks for adults compared to children during the winter haze episode in Xiantao. Moreover, the population health risks of PM<sub>2.5</sub>-bound metal(loid)s may not depend on the pollution levels but depend on the PM<sub>2.5</sub>-bound metal(loid)s concentrations. Other CAs, such as polycyclic aromatic hydrocarbons (PAHs) could also pose population health risks and need to be addressed in the future. The government and the public should pay more attention to the population health risks posed by PM<sub>2.5</sub>-bound metal(loid)s during a winter haze episode in JHP, central China.

**Supplementary Materials:** The following are available online at <http://www.mdpi.com/2073-4433/11/9/954/s1>, Supplementary Materials: Text S1: PM<sub>2.5</sub> Acidity, Sulfur, and Nitrogen Oxidation Ratios, Text S2: Enrichment Factor, Text S3: Chemical Mass Closure Method, Table S1: Summary of parameter values for population health risk assessment, Table S2: The mass concentrations (Mean  $\pm$  Standard deviation,  $\mu\text{g m}^{-3}$ ) of PM<sub>2.5</sub> and the corresponding species for the air mass back trajectory clusters during 13–23 January 2018 in Xiantao, Table S3: The ADPED ( $\text{mg kg}^{-1} \text{day}^{-1}$ ) of PM<sub>2.5</sub>-bound metal(loid)s through ingestion, inhalation, and dermal contact pathways for children and adults at different pollution levels, Figure S1: Time series of hourly meteorological parameter, including wind direction (WD), wind speed (WS), temperature (Temp.) relative humidity (RH), precipitation (Prec.), and visibility (Vis.) at Xiantao site in January 2018, Figure S2: Time series of trace gases ( $\text{SO}_2$  and  $\text{NO}_2$ ), SOR, and NOR during the sampling time at Xiantao site, Figure S3: The OC/EC ratios during the winter haze episode at Xiantao site, Figure S4: The (a) TE concentration and (b) correlations between EF and  $I_{\text{Geo}}$  at different pollution levels, Figure S3: The contamination levels for PM<sub>2.5</sub>-bound metal(loid)s at different pollution levels: (a) mild pollution, (b) moderate pollution, (c) heavy pollution, and (d) severe pollution, Figure S4: The population health carcinogenic risk and non-carcinogenic risk due to personal exposure to PM<sub>2.5</sub>-bound metal(loid)s for children and adults, respectively, at different pollution levels: (a) mild pollution, (b) moderate pollution, (c) heavy pollution, and (d) severe pollution.

**Author Contributions:** Conceptualization, data curation, and formal analysis, H.J.; methodology, H.J. and H.X.; investigation, X.L., H.X., D.C., P.Z., H.J., and X.Y.; writing—original draft, H.J.; validation and writing—review and editing, H.C.; supervision, resources, project administration, and funding acquisition, H.C. and Z.W. All authors have read and agreed to the published version of the manuscript.

**Funding:** This research was funded by the National Key R & D Program of China (Nos. 2017YFC0212603 and 2019YFB2102900) and the Natural Science Foundation of China (Grant No. 41673102).

**Acknowledgments:** We thank the engineer X.G. (Xinli Guo) from Wuhan Tianhong Instrument Co., Ltd. for the maintenance of sampling instrument. We are also grateful to the staff from Xiantao Municipal Ecological Environment Bureau for their support to the sampling work and the NOAA's Air Resources Laboratory for providing the HYSPLIT model and the READY website (<https://www.arl.noaa.gov/hysplit/>).

**Conflicts of Interest:** The authors declare no conflict of interest.

## References

1. Sun, Y.; Zhuang, G.; Tang, A.; Wang, Y.; An, Z. Chemical characteristics of PM<sub>2.5</sub> and PM<sub>10</sub> in haze-fog episodes in Beijing. *Environ. Sci. Technol.* **2006**, *40*, 3148–3155. [[CrossRef](#)] [[PubMed](#)]
2. Fiore, A.M.; Naik, V.; Spracklen, D.V.; Steiner, A.; Unger, N.; Prather, M.; Bergmann, D.; Cameron-Smith, P.J.; Cionni, I.; Collins, W.J.; et al. Cationic polymers and their therapeutic potential. *Chem. Soc. Rev.* **2012**, *41*, 6663–6683. [[CrossRef](#)] [[PubMed](#)]
3. Hamra, G.B.; Guha, N.; Cohen, A.; Laden, F.; Raaschou-Nielsen, O.; Samet, J.M.; Vineis, P.; Forastiere, F.; Saldiva, P.; Yorifuji, T.; et al. Outdoor particulate matter exposure and lung cancer: A systematic review and meta-analysis. *Environ. Health Perspect.* **2014**, *122*, 906–911. [[CrossRef](#)]
4. Loomis, D.; Grosse, Y.; Lauby-Secretan, B.; El Ghissassi, F.; Bouvard, V.; Benbrahim-Tallaa, L.; Guha, N.; Baan, R.; Mattock, H.; Straif, K. The carcinogenicity of outdoor air pollution. *Lancet Oncol.* **2013**, *14*, 1262–1263. [[CrossRef](#)]
5. Hu, X.; Zhang, Y.; Ding, Z.; Wang, T.; Lian, H.; Sun, Y.; Wu, J. Bioaccessibility and health risk of arsenic and heavy metals (Cd, Co, Cr, Cu, Ni, Pb, Zn and Mn) in TSP and PM<sub>2.5</sub> in Nanjing, China. *Atmos. Environ.* **2012**, *57*, 146–152. [[CrossRef](#)]
6. Zhang, R.; Wang, G.; Guo, S.; Zamora, M.L.; Ying, Q.; Lin, Y.; Wang, W.; Hu, M.; Wang, Y. Formation of Urban Fine Particulate Matter. *Chem. Rev.* **2015**, *115*, 3803–3855. [[CrossRef](#)]
7. Cakmak, S.; Dales, R.; Kauri, L.M.; Mahmud, M.; Van Ryswyk, K.; Vanos, J.; Liu, L.; Kumarathanan, P.; Thomson, E.; Vincent, R.; et al. Metal composition of fine particulate air pollution and acute changes in cardiorespiratory physiology. *Environ. Pollut.* **2014**, *189*, 208–214. [[CrossRef](#)]
8. Gavett, S.H.; Haykal-Coates, N.; Copeland, L.B.; Heinrich, J.; Gilmour, M.I. Metal composition of ambient PM<sub>2.5</sub> influences severity of allergic airways disease in mice. *Environ. Health Perspect.* **2003**, *111*, 1471–1477. [[CrossRef](#)]
9. Delfino, R.J.; Staimer, N.; Tjoa, T.; Gillen, D.L.; Polidori, A.; Arhami, M.; Kleinman, M.T.; Vaziri, N.D.; Longhurst, J.; Sioutas, C. Air pollution exposures and circulating biomarkers of effect in a susceptible population: Clues to potential causal component mixtures and mechanisms. *Environ. Health Perspect.* **2009**, *117*, 1232–1238. [[CrossRef](#)]
10. Elser, M.; Huang, R.; Wolf, R.; Slowik, J.G.; Wang, Q.; Canonaco, F.; Li, G.; Bozzetti, C.; Daellenbach, K.R.; Huang, Y.; et al. New insights into PM<sub>2.5</sub> chemical composition and sources in two major cities in China during extreme haze events using aerosol mass spectrometry. *Atmos. Chem. Phys.* **2016**, *3207*–3225. [[CrossRef](#)]
11. Shen, R.; Liu, Z.; Chen, X.; Wang, Y.; Wang, L.; Liu, Y.; Li, X. Atmospheric levels, variations, sources and health risk of PM<sub>2.5</sub>-bound polycyclic aromatic hydrocarbons during winter over the North China Plain. *Sci. Total Environ.* **2019**, *655*, 581–590. [[CrossRef](#)] [[PubMed](#)]
12. Xie, Y.; Liu, Z.; Wen, T.; Huang, X.; Liu, J.; Tang, G.; Yang, Y.; Li, X.; Shen, R.; Hu, B.; et al. Characteristics of chemical composition and seasonal variations of PM<sub>2.5</sub> in Shijiazhuang, China: Impact of primary emissions and secondary formation. *Sci. Total Environ.* **2019**, *677*, 215–229. [[CrossRef](#)] [[PubMed](#)]
13. Li, S.; Chang, M.; Li, H.; Cui, X.; Ma, L.Q. Chemosphere Chemical compositions and source apportionment of PM<sub>2.5</sub> during clear and hazy days: Seasonal changes and impacts of Youth Olympic Games. *Chemosphere* **2020**, *256*, 127163. [[CrossRef](#)] [[PubMed](#)]

14. Wei, N.; Xu, Z.; Wang, G.; Liu, W.; Zhouga, D.; Xiao, D.; Yao, J. Source apportionment of carbonaceous aerosols during haze days in Shanghai based on dual carbon isotopes. *J. Radioanal. Nucl. Chem.* **2019**. [[CrossRef](#)]
15. Qu, Y.; Gao, T.; Yang, C. Elemental characterization and source identification of the near-road PM<sub>2.5</sub> using EDXRF in Chengdu, China. *X-Ray Spectrom.* **2019**, *48*, 232–241. [[CrossRef](#)]
16. Wang, S.; Yin, S.; Zhang, R.; Yang, L.; Zhao, Q.; Zhang, L.; Yan, Q.; Jiang, N.; Tang, X. Insight into the formation of secondary inorganic aerosol based on high-time-resolution data during haze episodes and snowfall periods in Zhengzhou, China. *Sci. Total Environ.* **2019**, *660*, 47–56. [[CrossRef](#)]
17. Liu, J.; Li, J.; Vonwiller, M.; Liu, D.; Cheng, H.; Shen, K.; Salazar, G.; Agrios, K.; Zhang, Y.; He, Q.; et al. The importance of non-fossil sources in carbonaceous aerosols in a megacity of central China during the 2013 winter haze episode: A source apportionment constrained by radiocarbon and organic tracers. *Atmos. Environ.* **2016**, *144*, 60–68. [[CrossRef](#)]
18. Jiang, H.; Xiao, H.; Song, H.; Liu, J.; Wang, T.; Cheng, H.; Wang, Z. A long-lasting winter haze episode in Xiangyang, Central China: Pollution characteristics, chemical composition, and health risk assessment. *Aerosol Air Qual. Res.* **2020**, *20*. [[CrossRef](#)]
19. Qu, C.; Xing, X.; Albanese, S.; Doherty, A.; Huang, H.; Lima, A.; Qi, S.; De Vivo, B. Spatial and seasonal variations of atmospheric organochlorine pesticides along the plain-mountain transect in central China: Regional source vs. long-range transport and air-soil exchange. *Atmos. Environ.* **2015**, *122*, 31–40. [[CrossRef](#)]
20. Liu, R.; Ma, Z.; Liu, Y.; Shao, Y.; Zhao, W.; Bi, J. Spatiotemporal distributions of surface ozone levels in China from 2005 to 2017: A machine learning approach. *Environ. Int.* **2020**, *142*, 105823. [[CrossRef](#)]
21. Liu, Q.; Baumgartner, J.; Zhang, Y.; Schauer, J.J. Source apportionment of Beijing air pollution during a severe winter haze event and associated pro-inflammatory responses in lung epithelial cells. *Atmos. Environ.* **2016**, *126*, 28–35. [[CrossRef](#)]
22. Cheng, H.; Gong, W.; Wang, Z.; Zhang, F.; Wang, X.; Lv, X.; Liu, J.; Fu, X.; Zhang, G. Ionic composition of submicron particles (PM<sub>1.0</sub>) during the long-lasting haze period in January 2013 in Wuhan, central China.pdf. *J. Environ. Sci.* **2014**, *26*, 810–817. [[CrossRef](#)]
23. Zhang, F.; Cheng, H.R.; Wang, Z.W.; Lv, X.P.; Zhu, Z.M.; Zhang, G.; Wang, X.M. Fine particles (PM<sub>2.5</sub>) at a CAWNET background site in Central China: Chemical compositions, seasonal variations and regional pollution events. *Atmos. Environ.* **2014**, *86*, 193–202. [[CrossRef](#)]
24. Zhang, F.; Wang, Z.W.; Cheng, H.R.; Lv, X.P.; Gong, W.; Wang, X.M.; Zhang, G. Seasonal variations and chemical characteristics of PM<sub>2.5</sub> in Wuhan, Central China. *Sci. Total Environ.* **2015**, *518*, 97–105. [[CrossRef](#)] [[PubMed](#)]
25. Lyu, X.-P.; Wang, Z.-W.; Cheng, H.-R.; Zhang, F.; Zhang, G.; Wang, X.-M.; Ling, Z.-H.; Wang, N. Chemical characteristics of submicron particulates (PM<sub>1.0</sub>) in Wuhan, Central China. *Atmos. Res.* **2015**, *161*, 169–178. [[CrossRef](#)]
26. Cai, K.; Li, C.; Na, S. Spatial Distribution, Pollution Source, and Health Risk Assessment of Heavy Metals in Atmospheric Depositions: A Case Study from the Sustainable City of Shijiazhuang, China. *Atmosphere* **2019**, *10*, 222. [[CrossRef](#)]
27. State Environmental Protection Bureau. *Background Values of Soil Elements in China*, 1st ed.; China Environmental Monitoring Station, Ed.; China Environmental Science Press: Beijing, China, 1990.
28. Li, N.; Han, W.; Wei, X.; Shen, M.; Sun, S. Chemical characteristics and human health assessment of PM<sub>1</sub> during the Chinese Spring Festival in Changchun, Northeast China. *Atmos. Pollut. Res.* **2019**, *10*, 1823–1831. [[CrossRef](#)]
29. Massey, D.D.; Kulshrestha, A.; Taneja, A. Particulate matter concentrations and their related metal toxicity in rural residential environment of semi-arid region of India. *Atmos. Environ.* **2013**, *67*, 278–286. [[CrossRef](#)]
30. US Environmental Protection Agency. *Exposure Factors Handbook: 2011 Edition*; US Environmental Protection Agency: Washington, DC, USA, 2011; EPA/600/R-090/052F.
31. Wang, N.; Zhao, X.; Wang, J.; Yin, B.; Geng, C.; Niu, D. Chemical Composition of PM<sub>2.5</sub> and Its Impact on Inhalation Health Risk Evaluation in a City with Light Industry in Central China. *Atmosphere* **2020**, *11*, 340. [[CrossRef](#)]
32. Griselda, J.; Mar, R.; Antonio, A.; Guzman, E.; Guarnaccia, C.; Mart, S.; Lara, C.; Rangel, M.; Hern, G.; Lozada, C.; et al. Trace Metal Content and Health Risk Assessment of PM<sub>10</sub> in an Urban Environment of León, Mexico. *Atmosphere* **2019**, *10*, 573. [[CrossRef](#)]

33. International Agency for Research on Cancer. *Agents Classified by the IARC Monographs*; World Health Organization: Geneva, Switzerland, 2020; Volume 1-116.
34. Roy, D.; Singh, G.; Seo, Y.C. Carcinogenic and non-carcinogenic risks from PM<sub>10</sub>- and PM<sub>2.5</sub>-Bound metals in a critically polluted coal mining area. *Atmos. Pollut. Res.* **2019**, *10*, 1964–1975. [[CrossRef](#)]
35. Xue, H.; Liu, G.; Zhang, H.; Hu, R.; Wang, X. Similarities and differences in PM<sub>10</sub> and PM<sub>2.5</sub> concentrations, chemical compositions and sources in Hefei City, China. *Chemosphere* **2019**, *220*, 760–765. [[CrossRef](#)]
36. Mao, Y.; Hu, T.; Shi, M.; Cheng, C.; Liu, W.; Zhang, J. PM<sub>2.5</sub>-bound PAHs during a winter haze episode in a typical mining city, central China: Characteristics, influencing parameters, and sources. *Atmos. Pollut. Res.* **2020**, *11*, 131–140. [[CrossRef](#)]
37. Giorgiana Galon-Negru, A.; Iulian Olariu, R.; Arsene, C. Chemical characteristics of size-resolved atmospheric aerosols in Iasi, north-eastern Romania: Nitrogen-containing inorganic compounds control aerosol chemistry in the area. *Atmos. Chem. Phys.* **2018**, *18*, 5879–5904. [[CrossRef](#)]
38. Akyüz, M.; Çabuk, H. Meteorological variations of PM<sub>2.5</sub>/PM<sub>10</sub> concentrations and particle-associated polycyclic aromatic hydrocarbons in the atmospheric environment of Zonguldak, Turkey. *J. Hazard. Mater.* **2009**, *170*, 13–21. [[CrossRef](#)] [[PubMed](#)]
39. Modaihsh, A.S.; Al-Barakah, F.N.; Nadeem, M.E.A.; Mahjoub, M.O. Spatial and Temporal Variations of the Particulate Matter in Riyadh City, Saudi Arabia. *J. Environ. Prot.* **2015**, *6*, 1293–1307. [[CrossRef](#)]
40. Zhong, S.; Zhang, L.; Jiang, X.; Gao, P. Comparison of chemical composition and airborne bacterial community structure in PM<sub>2.5</sub> during haze and non-haze days in the winter in Guilin, China. *Sci. Total Environ.* **2019**, *655*, 202–210. [[CrossRef](#)] [[PubMed](#)]
41. Khanna, I.; Khare, M.; Gargava, P.; Khan, A.A. Effect of PM<sub>2.5</sub> chemical constituents on atmospheric visibility impairment.pdf. *J. Air Waste Manag. Assoc.* **2018**, *68*, 430–437. [[CrossRef](#)]
42. Chow, J.C.; Fujita, E.M.; Watson, J.G.; Lu, Z.; Lawson, D.R. Evaluation of Filter-based Aerosol Measurements During the 1987 Southern California Air Quality Study. *Environ. Monit. Assess.* **1994**, *87*, 49–80. [[CrossRef](#)]
43. Wang, Y.; Zhuang, G.; Tang, A.; Yuan, H.; Sun, Y.; Chen, S.; Zheng, A. The ion chemistry and the source of PM<sub>2.5</sub> aerosol in Beijing. *Atmos. Environ.* **2005**, *39*, 3771–3784. [[CrossRef](#)]
44. Arimoto, R.; Duce, R.A.; Savoie, D.L.; Prospero, J.M.; Talbot, R.; Cullen, J.D.; Tomza, U.; Lewis, N.F.; Ray, B.J. Relationships among aerosol constituents from Asia and the North Pacific during PEM-West A. *J. Geophys. Res.* **1996**, *101*, 2011–2023. [[CrossRef](#)]
45. Yin, L.; Niu, Z.; Chen, X.; Chen, J.; Zhang, F.; Xu, L. Characteristics of water-soluble inorganic ions in PM<sub>2.5</sub> and PM<sub>2.5–10</sub> in the coastal urban agglomeration along the Western Taiwan Strait Region, China. *Environ. Sci. Pollut. Res.* **2014**, *21*, 5141–5156. [[CrossRef](#)] [[PubMed](#)]
46. Yang, S.; Ma, Y.L.; Duan, F.K.; He, K.B.; Wang, L.T.; Wei, Z.; Zhu, L.D.; Ma, T.; Li, H.; Ye, S.Q. Characteristics and formation of typical winter haze in Handan, one of the most polluted cities in China. *Sci. Total Environ.* **2018**, *613–614*, 1367–1375. [[CrossRef](#)] [[PubMed](#)]
47. Feng, J.; Yu, H.; Mi, K.; Su, X.; Li, Y.; Li, Q.; Sun, J. One year study of PM<sub>2.5</sub> in Xinxiang city, North China: Seasonal characteristics, climate impact and source. *Ecotoxicol. Environ. Saf.* **2018**, *154*, 75–83. [[CrossRef](#)]
48. Pachauri, T.; Satsangi, A.; Singla, V.; Lakhani, A.; Maharaj Kumari, K. Characteristics and sources of carbonaceous aerosols in PM<sub>2.5</sub> during wintertime in Agra, India. *Aerosol Air Qual. Res.* **2013**, *13*, 977–991. [[CrossRef](#)]
49. Bressi, M.; Sciare, J.; Ghersi, V.; Mihalopoulos, N.; Petit, J.-E.; Nicolas, J.B.; Moukhtar, S.; Rosso, A.; Féron, A.; Bonnaire, N.; et al. Sources and geographical origins of fine aerosols in Paris (France). *Atmos. Chem. Phys.* **2014**, *14*, 8813–8839. [[CrossRef](#)]
50. Mamane, Y.; Perrino, C.; Youssef, O.; Catrambone, M. Source characterization of fine and coarse particles at the East Mediterranean coast. *Atmos. Environ.* **2008**, *42*, 6114–6130. [[CrossRef](#)]
51. Zhang, R.; Jing, J.; Tao, J.; Hsu, S.-C.; Wang, G.; Cao, J.; Lee, C.S.L.; Zhu, L.; Chen, Z.; Zhao, Y.; et al. Chemical characterization and source apportionment of PM<sub>2.5</sub> in Beijing: Seasonal perspective. *Atmos. Chem. Phys.* **2013**, *13*, 7053–7074. [[CrossRef](#)]
52. Kong, S.F.; Li, L.; Li, X.X.; Yin, Y.; Chen, K.; Liu, D.T.; Yuan, L.; Zhang, Y.J.; Shan, Y.P.; Ji, Y.Q. The impacts of firework burning at the Chinese Spring Festival on air quality: Insights of tracers, source evolution and aging processes. *Atmos. Chem. Phys.* **2015**, *15*, 2167–2184. [[CrossRef](#)]

53. Zheng, H.; Kong, S.; Wu, F.; Cheng, Y.; Niu, Z.; Zheng, S.; Yang, G.; Yao, L.; Yan, Q.; Wu, J.; et al. Intra-regional transport of black carbon between the south edge of the North China Plain and central China during winter haze episodes. *Atmos. Chem. Phys.* **2019**, *19*, 4499–4516. [[CrossRef](#)]
54. Izhar, S.; Goel, A.; Chakraborty, A.; Gupta, T. Annual trends in occurrence of submicron particles in ambient air and health risk posed by particle bound metals. *Chemosphere* **2016**, *146*, 582–590. [[CrossRef](#)] [[PubMed](#)]



© 2020 by the authors. Licensee MDPI, Basel, Switzerland. This article is an open access article distributed under the terms and conditions of the Creative Commons Attribution (CC BY) license (<http://creativecommons.org/licenses/by/4.0/>).